DOI: 10.1002/chem.200801911

Solid-State Gas Sensors Developed from Functional Difluoroboradiazaindacene Dyes

Raymond Ziessel,*[a] Gilles Ulrich,[a] Anthony Harriman,[b] Mohammed A. H. Alamiry,[b] Beverly Stewart,[b] and Pascal Retailleau[c]

Abstract: This article describes the synthesis and characterization of several new difluoroboradiazaindacene (BODIPY™) dyes functionalized at the central 8-position by a phenyliodo, phenylheptynoate or phenylheptynoic fragment and at the 3- or 3/5-position(s) by 4-dimethylaminophenylstyryl residue(s). Single-crystal structural determinations confirm the planarity of the dyes, while the absorption and fluorescence spectroscopic properties are highly sensitive to the state of protonation (or alkylation) of the terminal anilino donor group(s). Reversible color tuning from green to blue for absorption and from colorless (i.e., near-IR region) to red for fluorescence is obtained on successive addition of acid and base. The difunctionalized derivative is especially interesting in this respect and shows two well-resolved pK_a values of 5.10 and 3.04 in acetonitrile. Addition of the first proton causes only small spectral changes and deactivates the molecule towards addition of the second proton. It is this latter step that accommodates the large change in absorption and emission properties, due to the reversible extinction of the intramolecular charge-transfer character inherent to this type of dye. The main focus of the work is the covalent anchoring of the dyes to inert, porous polyacrylate beads so as to form a solid-state sensor suitable for analysis of gases or flowing liquids. The final material is highly stable—its performance is undiminished after more than one year—and fully reversible over many cycles. The sensitivity is such that reactions can be followed by the naked eye and the detection limit is about 600 ppb for HCl and about 80 ppb for ammonia. Trace amounts of diphosgene can be detected, as can alkylating agents. The sensing action is indiscriminate and also operates when the beads are dispersed in aqueous media.

Keywords: analytical methods · dyes/pigments · fluorescence · functional beads · sensors

Introduction

A wide variety of chemical sensors capable of monitoring trace amounts of atmosphere-borne pollutants and various analytes at ambient temperature have been described and tested under rigorous conditions.[1,2] The more advanced systems tend to use polymer films loaded with dyes[3] that undergo well-defined color changes in the presence of the target substrate and make use of common dyes such as metal-free porphyrins,[4–6] Phenol Red,[7] oxazines,[8] Reichardt dyes,[9] sulfophthalein,[10] or Nile Red.[11] In certain cases, polymeric materials such as poly(2-methoxyaniline),[12] poly(aniline),[13] or poly(pyrrole)[14] play active roles in the sensing process, rather than simply providing an inert support. The vast majority of these systems employ optical absorption spectral changes to provide the monitoring signal, although related systems are known in which the sensing action is triggered by a change in fluorescence intensity and/or spectral distribution.[3,8] A persistent problem encountered in many hybrid materials, such as dyes entrapped in

[a] Dr. R. Ziessel, Dr. G. Ulrich
Laboratoire de Chimie Moléculaire
Ecole Européenne de Chimie, Polymères et Matériaux
CNRS, 25 rue Becquerel, 67087 Strasbourg Cedex 02 (France)
Fax: (+33) 3-90-24-26-89
E-mail: ziessel@chimie.u-strasbg.fr

[b] Prof. A. Harriman, Dr. M. A. H. Alamiry, B. Stewart
Molecular Photonics Laboratory
School of Natural Sciences, Bedson Building
University of Newcastle
Newcastle upon Tyne, NE1 7RU (United Kingdom)

[c] Dr. P. Retailleau
Laboratoire de Cristallochimie
ICSN—CNRS, Bât 27 1 avenue de la Terrasse
91198 Gif-sur-Yvette, Cedex (France)

Supporting information for this article is available on the WWW under http://dx.doi.org/10.1002/chem.200801911.

sol–gels,[7] copolymers,[6] or composite films,[5] relates to the dye leaching from the host material[15] and this situation serves to limit the shelf life of the device. It also poses severe problems for the measurement of low concentrations of substrate, especially when used in the fluorescence mode. The only logical solution to this particular problem is to attach the dye to the host by way of robust covalent linkages.

In searching for suitable chromophores that could be adapted for the simultaneous measurement of absorption and fluorescence changes, such behavior is taken as being representative of the simplest form of orthogonal detection, imposed by the presence of acids, bases, or toxins such as phosgene, our attention has been drawn to the difluoroboraindacenes (BODIPY) class of dyes.[16,17] These materials, which are stable, easily functionalized and highly fluorescent, have been developed as laser dyes,[18] selective fluorescent tags,[19] molecular sensors,[20] donor–acceptor dyads,[21] solar concentrators,[22] and components for electroluminescent devices.[23] Of particular interest is the realization that their optical properties can be fine-tuned by chemical modification of the organic core,[24] or at the boron center.[25] For instance, the attachment of electron-rich residues at the 8-position, or at the boron atom, has little effect on the absorption spectral profile. In contrast, grafting unsaturated groups to the 2,6-positions serves to red-shift the absorption maximum by about 50 nm for each attachment.[26] A spectacular hypsochromic shift accompanies substitution at the 3,5-positions by vinylic[27,28] or acetylenic fragments.[29] Moreover, BODIPY-based dyes enter readily into charge-transfer processes such that their absorption and emission properties can be further adjusted by controlling the electron affinity of appended donor and/or acceptor groups.[30,31] This last realization forms the basis of the operating mechanism for the sensors reported here.

We are particularly interested in the concept of monitoring the concentration of species present as contaminants in a flowing effluent stream, either gaseous or liquid. This is best achieved using a porous support functionalized with a predetermined loading of the sensor. The sensor must be firmly attached to the support and undergo distinctive and reversible color changes that themselves lead to marked differences in the fluorescence properties. We are aware that a tremendous wealth of information has accumulated over the past few decades regarding the design of chemical sensors for the in situ monitoring of analytes, although most refer to static liquids, and protocols have been established for testing such materials under various conditions.[1–3] In developing the present system, we have given considerable attention to the sensing mechanism and have set out to ensure orthogonal detection. In particular, the color change has been carefully optimized for maximum visibility, while the fluorescence changes are equally dramatic. The work should be considered as being "proof-of-concept" for which future rational modifications would allow for the detection of specific substrates by building the chromophore into a suitable receptor site using well-known strategies.

Abstract in French: *Ce manuscrit décrit la synthèse et la caractérisation de nouvelles sondes fluorescentes communément appelées BODIPY qui ont été ciselées en position centrale par un groupe phényl-iodo, phénylheptynoate ou phénylheptanoic acide et en positions 5 ou 3/5 avec des fragments 4-diméthylaminostyryle. Ces derniers fragments favorisent une excellente conjugaison qui est à l'origine de la couleur verte des sondes. Des structures moléculaires obtenues par diffraction aux rayon X sur monocristal confirment la planarité des ces objets, tandis que les propriétés d'absorption et de fluorescence sont sensibles à la protonation ou l'alkylation des groupements aminés terminaux. Un changement de couleur réversible du vert au bleu par absorption et de l'invisible au rouge en fluorescence est obtenu en présence d'un flux d'air pimenté avec des traces d'acides. La réversibilité est observée en présence de traces de base. Le dérivé di-fonctionnalisé est particulièrement intéressant dans la mesure ou deux pKa sont bien résolus à 5,10 et 3,04 unités dans l'acétonitrile. L'addition du premier proton induits des changements spectroscopiques modestes et diminue la basicité du deuxième groupe amino. Cette dernière protonation induit des changements majeurs en absorption et émission et inhibe le transfert de charge intramoléculaire. L'intérêt majeur de ces sondes réside dans leur potentiel d'être lié de façon covalente à des billes de polymères et d'utiliser ces billes pour la détection d'éléments toxiques dans des effluents gazeux. En particulier il a été démontré que la détection visuelle de trace de HCl (environ 600 ppb) ou d'ammoniaque (environ 80 ppb) est possible sans l'utilisation de systèmes de détection particuliers. De façon similaire des traces de diphosgène et d'autre agent vésicant et alkylant est possible. Ces systèmes sont très stables (durée supérieure à un an) et fonctionnent également en phase aqueuse. Aucune sélectivité de détection n'a été obtenue mais conceptuellement les systèmes sont particulièrement sensibles et peuvent être modifiés à façon.*

Results and Discussion

Synthesis and X-ray characterization: Taking account of the arguments raised above, and making due allowance for related demands needed for the design of a viable orthogonal sensor, dyes **1** and **2** were designed. Dye **1** is regarded as a reference compound with which to judge the significance of increased conjugation, dye **2** is intended as the prototype with which to examine our general strategy, while the iodobenzene unit attached at the *meso*-position will provide the linkage to the porous polymer beads. These dyes were synthesized from the 8-iodophenyl-1,3,5,7-tetramethyl-4-bora-3a,4a-diaza-*s*-indacene derivative by condensation with 4-dimethylaminobenzaldehyde by using piperidine as catalyst.[27] Both the monosubstituted dye, **1**, which is blue, and the disubstituted compound, **2**, this being green, were isolated by column chromatography.[27a] Alkylation of the dimethyl-

amino groups present in **2** is kinetically controlled and the use of CH_3I in acetonitrile gives rise to both the mono-alkylated compound **3a** (green, 20%) and the dialkylated compound **3b** (blue, 55%). The alkylated dyes are stable for several weeks, but show some degradation after long-term storage in air at room temperature. Dyes **4** and **5** are equipped with an alternative anchor. We draw attention to the similarity between **1** and BODIPY-dyes reported by Boens et al.[28] The main points of interest in our work concern attaching the dye to an inert support and examining the advantages of equipping the dye with two identical vinyl arms.

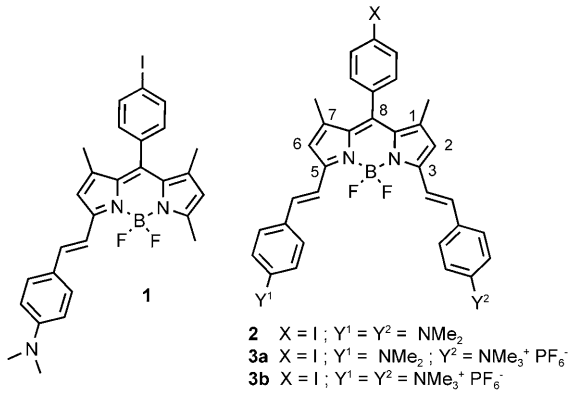

Compound **1** crystallizes in the monoclinic space group, $P2_1$, whereas crystals of **2** fall within the centrosymmetric triclinic space group. The two pyrrole rings that make up the BODIPY core are quasi planar, for both compounds, with their mean deviations from the least-squares molecular plane being 0.021 and 0.067 Å, respectively. The structure of **2** is slightly distorted, because the anilino substituents act as levers, with the maximum deviation from planarity of 0.12 and −0.11 Å being observed for C5 and C7, respectively (from one outermost pyrrole ring). The iodobenzene unit lies orthogonal to the BODIPY nucleus due to the presence of methyl groups on either side, with the dihedral angles being 86.4 and 83.3° for **1** and **2**, respectively (Figure 1). This orthogonal arrangement is a common feature of structures computed at various levels for all of the compounds **1**–**5**; the average dihedral angle is calculated at 85°.

In both **1** and **2**, the bond lengths and angles around the boron atom are as might be expected on the basis of other BODIPY structures.[32,33] The effect of the vinyl group can be seen clearly by comparing the bond lengths for C4−N1 and C5−N2 and for C1−N1 and C8−N2 (Table S1 in the Supporting Information). Note that the I1−C4A bond lengths are in compliance with the mean value 2.099 (0.026) Å found from a survey of 1075 structures contained in the CCDC database. The eleven atoms of the anilino subunits are essentially co-planar in each structure, with mean deviations from the respective least-squares molecular plane of 0.035 Å in **1** and 0.04 and 0.08 Å in **2**. The respective

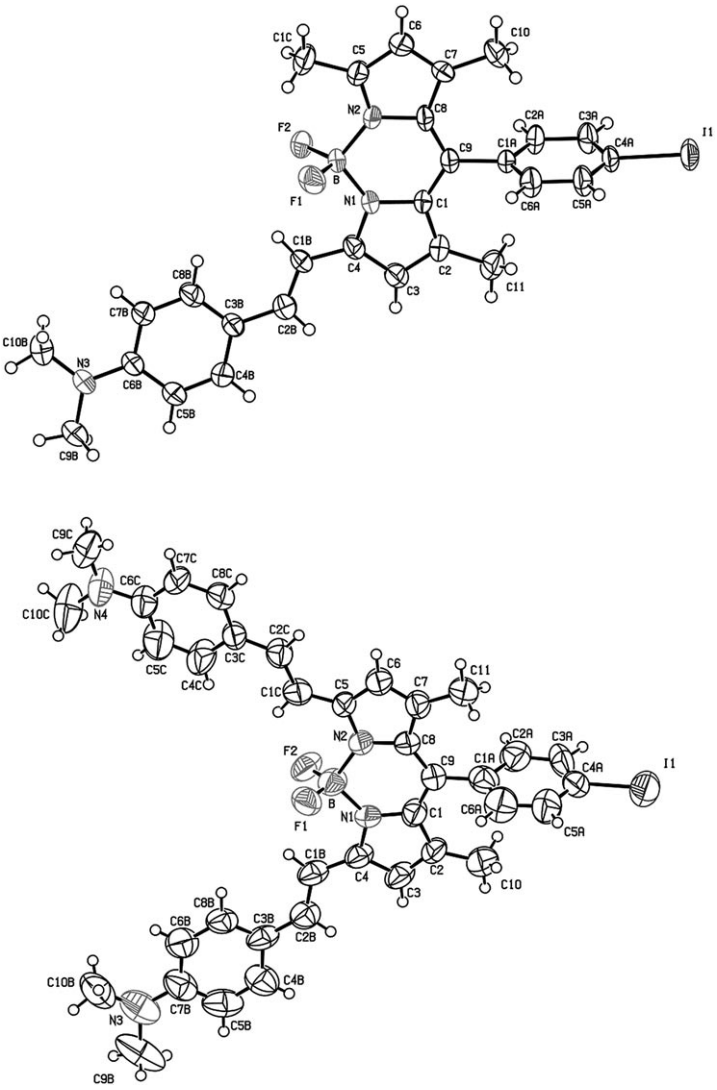

Figure 1. Top: ORTEP view of compound **1**. Bottom: ORTEP view of compound **2**. Displacement ellipsoids are drawn at the 50% probability level and H atoms are shown as small spheres of arbitrary radii.

dihedral angles between these mean planes and the BODIPY nucleus are slightly twisted (10.3° for **1**; 12.5 and 17.3° for **2**). In the monosubstituted derivative **1**, the anilino subunit is almost aligned with the BODIPY nucleus. However, in the V-shaped molecule **2** these subunits are directed above and below the mean plane of the BODIPY platform, making approximate angles of −10 and 15°, respectively.

The molecular arrangement in the crystal structure determined for **1** is set primarily by directional iodine···methyl intermolecular interactions of 3.62 Å along the $20\bar{1}$ direction, linking one molecule at general position x, y, z to two molecules at positions $(1-x, y-1/2, -z)$ and $(1-x, y+1/2, -z)$. Cohesion is reinforced through short-range interactions between F2 and hydrogen atoms located at C6A and C9B with respective positions #i $(x-1, y, z)$ and #ii $(-1-x, y+1/2, 1-z)$. Additional secondary interactions include C···H π-ring edge-to-face interactions (e.g., between C5A···H5A and the

central six-membered ring at position $1+x$, y, z (distance 3.12 Å and angle 162.3°), and between C7B···H7B and the aniline ring at position #ii (distance 2.98 Å and angle 163.3°)). The crystal packing can be viewed as chains of tetrameric units (see Supporting Information, Figure S1a), with the iodobenzene–BODIPY moieties stacking along the *b* screw axis, appearing head-to-head around position $z=0$, and the anilino subunits being edge-to-face linked at $z=1/2$ (see Supporting Information, Figure S1b).

For compound **2**, the V-shaped molecules are intertwined across an inversion center (the angle of ca. 50° between the two arms is sufficient for insertion of a symmetry-related molecule) and lie parallel to the plane (1 2 0), with all iodobenzene groups aligned along the same direction. The molecules are arranged with an inclination of 31.1° and without π–π overlap. This gives the appearance of a staircase-like pattern, with the aniline subunits as the steps and the iodobenzene units as banisters. Adjacent staircases propagating along the *c* direction display zigzag sheets (see Supporting Information Figure S2). The most noticeable stabilization of the molecular packing can be attributed to a C···H interaction, with a contact distance of 2.61 Å, between the methyl C9B of the aniline molecule at position $-x$, $-y$, $1-z$ and the central BODIPY ring. The aniline rings stack over the vinyl groups, thereby augmenting the overall stabilization of the structure. We note in passing that single crystals of **1** and **2** are nonfluorescent at ambient temperature. This is in marked contrast to the ready detection of emission from solutions of these dyes and indicates that the crystalline material is subjected to strong fluorescence quenching by short-range interactions.

Molecular modeling studies made for the various compounds clearly indicate a *trans* arrangement of the vinyl double bond, as observed by both X-ray diffraction and ^{1}H NMR spectroscopy; calculations made with the STO 3G* basis set conclude that the *trans* form of **1** is more stable than the *cis* form by 22.6 kJ mol^{-1}. As expected, a high barrier ($E_a=215$ kJ mol^{-1}) is calculated for rotation around the vinyl double bond (see Supporting Information Figure S3). The modeling work indicates that the styryl residue in the *trans* form prefers to align with the dipyrrin nucleus, there being two such geometric arrangements, each of comparable energy, separated by a barrier of 6 ± 2 kJ mol^{-1}. These two stable structures have closely comparable excitation energies and are inter-converted by rotation around the C–C bond linking the vinyl group to the pyrrole ring (see Supporting Information Figure S4). The excitation energy computed for the *cis* form is only 10 kJ mol^{-1} higher than that of the *trans* form.

Spectral properties: Each of the compounds displays several strong π–π* absorption transitions in the 300–750 nm region; the lowest energy absorption maxima (λ_{abs}) and molar absorption coefficients (ε_{max}) are collected in Table 1. Dye **1** has similar spectroscopic features to those exhibited by the analogous compound lacking the iodine substituent.[30] Particular attention should be paid to the strong absorption centered at around 700 nm as found for **2**, since this is the key to understanding much of the ensuing analytical chemistry. This transition contains an important contribution from intramolecular charge-transfer effects arising from interaction between the amino donor and the BODIPY-based acceptor. Such an effect favors establishing quinoidal resonance structures for charge delocalization and has been studied in detail for a compound closely related to **1**.[28] Alkylation of both amino groups induces a strong hypsochromic shift and the charge-transfer absorption band disappears, since the N lone pair is no longer available to act as a donor. Consequently, the absorption maximum for **3b** is found at 617 nm. Interestingly, the mono-alkylated compound **3a** exhibits a blue shift of 30 nm for absorption and 10 nm for emission spectra relative to **2** (Table 1). To the best of our knowledge, these are the first ammonium-type BODIPY derivatives to be well characterized. The absorption maxima recorded for **4** and **5**, which differ only in respect of the nature of the *meso* substituent, are in the far-red region and, as expected, are strongly reminiscent of **2** (Table 1). This latter finding can be used to raise the idea that attaching the dye to an inert support is unlikely to perturb the photophysical properties.

Table 1. Spectroscopic data for the compounds measured at room temperature.[a]

Property	**1**	**2**[b]	**3a**	**3b**	**4**	**5**
λ_{abs} [nm^{-1}]	596	706	675	617	703	702
ε_{max} [M^{-1} cm^{-1}]	78000	83000	70000	60800 [c]	81800	82000
λ_{flu} [nm^{-1}]	639	767	756	630	762	762
τ_F [ns^{-1}]	3.2	3.0	1.2	8.0	3.6	3.6
ϕ_F	0.85	0.18	0.07	0.62	0.21	0.22
k_{RAD} [10^7 s^{-1}][d]	27	6	6	8	6	6
k_{NR} [10^7 s^{-1}][d]	5	27	77	5	22	22

[a] Determined in CH_2Cl_2, except for **3b** where measurements were made in CH_3CN. [b] Same ε and λ were measured after addition of a drop of triethylamine or acetic acid. [c] A second peak lies at 562 nm ($\varepsilon_{max}=36{,}700$ M^{-1} cm^{-1}). [d] Calculated using the following equations: $k_{RAD}=\phi_F/\tau_F$, $k_{NR}=(1-\phi_F)/\tau_F$.

The substituents affect the molecular polarizability, as indicated in Figure 2. Relative to the phenyl analogue, both the *N*,*N*-dimethylanilino group and the corresponding *N*,*N*,*N*-trimethylammonium derivative possess considerably higher polarizability, with the former being the highest. It is crucial for the design of an intelligent sensor that these groups work in a cooperative fashion so as to amplify the spectral changes that accompany protonation or alkylation

Figure 2. Contour plots showing the computed molecular polarizability for **2** (left-hand side), **3a** (center) and **3b** (right-hand side). Light = Positive: Dark = Negative.

of the donor. Thus, the vinyl residue is intended to increase the conjugation length and thereby push the absorption and fluorescence maxima to longer wavelength. The anilino donor is intended to shift these maxima, especially the fluorescence band, to lower energy by way of charge-transfer interactions and to provide the reactive site. The ammonium cation is intended to serve the dual purpose of removing the charge-transfer interactions and shortening the conjugation length by an inductive effect. It is only by combining these various phenomena that the full impact of the sensor will become apparent. The polarizability plots indicate that this level of mutual co-operation is viable. Related displays of the molecular HOMOs and LUMOs are given in the Supporting Information (Figure S5).

Each new derivative fluoresces in fluid solution at ambient temperature and the emission maxima (λ_{flu}) recorded in CH_2Cl_2 are collected in Table 1. For **1**, the Stokes' shift is 1130 cm^{-1}, which is indicative of the excited state showing increased charge-transfer character, while the fluorescence quantum yield (ϕ_F) is rather high. The singlet-excited state decays by mono-exponential kinetics with a lifetime (τ_F) of 3.2 ns. For this compound, the radiative rate constant (k_{RAD}) has a value of 2.7×10^8 s^{-1}; this value is in reasonable agreement with other BODIPY derivatives bearing a single vinyl group at the 2-position. Indeed, the photophysical properties recorded for **1** are in good accord with those reported for a closely-related BODIPY-based dye, taking due account of the pronounced solvent dependence reported previously.[28] The rate constant for nonradiative decay (k_{NR}) is relatively unimportant for this compound. Increasing the conjugation length, as for **2**, pushes the emission wavelength to lower energy, but has no effect on the Stokes' shift. There is a marked decrease in the fluorescence quantum yield relative to **1**, a sharp drop in k_{RAD} and a corresponding increase in k_{NR}. Compounds **4** and **5** exhibit ϕ_F and τ_F values that remain comparable to those observed for **2**, indicating that the iodine atom is too remote to influence the photophysical properties. The Stokes' shifts measured for **4** and **5** are also similar to that of **2**, as might be expected if the nature of the fluorophore remains constant (Table 1).

It is informative at this point to make a critical comparison of the photophysical properties of **1** and **2** and subsequently to broaden the discussion to include **3a**. On the basis of the detailed studies made for somewhat similar derivatives, it can be argued that the excited-singlet state of **1** has considerably more polar character than the corresponding ground state. The measured k_{RAD} and k_{NR} values can be taken as referring to decay of a charge-transfer state, with the actual values being related to the magnitude of the change in dipole moment that occurs on excitation. An increased dipole moment, as realized by moving to a solvent with higher dielectric constant, will increase k_{NR} and decrease k_{RAD}. This is also what happens when the second electron-donating arm is added to **1**. Here, the dipole moment remains unaffected, but the excitation energy, defined as the intersection point between normalized absorption and fluorescence spectra after conversion from wavelength to wavenumber, decreases markedly. It is this decrease that leads to an enhancement of k_{NR}, in agreement with the energy-gap law,[34] and the expected reduction in k_{RAD}. The reduced excitation energy is clearly a consequence of the longer effective conjugation length and is not to be confused with an increased change in dipole moment.

The absorption and emission maxima recorded for **3a** in CH_2Cl_2 fall between those determined for **1** and **2**. Compound **3a** has two vinyl substituents, but only one terminal donor group. The effect of removing one donor group is to push λ_{max} from 706 to 675 nm and to lower λ_{flu} from 767 to 756 nm. This is due to the inductive effect of the ammonium ion and serves to lower the effective conjugation length. The Stokes' shift is 1590 cm^{-1} and is the highest of all the compounds described here. The dipole moment is raised relative to **1**, because the BODIPY-based acceptor is made more electron affinic by the second vinyl substituent. In **2**, the dipole moment is kept modest by having two donors competing for the same acceptor. The derived k_{RAD} and k_{NR} values now represent a compromise between the increased dipole moment (lowering k_{RAD} but raising k_{NR}) and the increased excitation energy (raising k_{RAD} but lowering k_{NR}).

On removing the remaining terminal donor, as for **3b**, the absorption and emission spectra move to higher energy and the Stokes' shift falls to 335 cm^{-1}. This value indicates the absence of a significant geometry change on excitation and is consistent with the lack of intramolecular charge-transfer character. Both ϕ_F and τ_F increase to values typical of conventional BODIPY-based dyes, allowing for the relatively low excitation energy. It is important to note that whereas fluorescence from **2** is outside of the visible region, that from **3b** is clearly apparent to the naked eye. It should also be emphasized that the vinyl groups inherent to **2** do not provide extra decay channels, such as isomerization.

pH Titration: During the pH titration of **1** in acetonitrile, with HCl as the proton source, the absorption maximum undergoes a hypsochromic shift from 597 to 553 nm, the fluorescence maximum moves from 717 to 561 nm, and the fluorescence quantum yield increases from 0.09 to 1.0 upon protonation of the terminal donor N atom. Under the same conditions, k_{RAD} increases from 7.5×10^7 to 2.4×10^8 s^{-1}. On the assumption that HCl is fully dissociated in acetonitrile, the titration data correspond to a pK_a of 2.25 for the donor N atom. We have been concerned with extending this pH titration to **2**, knowing that N-alkylation occurs in two well-resolved steps. Control experiments confirmed that addition of acid (i.e., HCl or CF_3COOH) had no effect on the absorption and fluorescence spectra recorded for **3b** in acetonitrile or CH_2Cl_2.

Addition of excess HCl to **2** in CH_3CN results in a hypsochromic shift from 700 to 620 nm, this absorption maximum being reminiscent of that found for **3b**. The fluorescence maximum shows a similar shift, moving from 780 to 630 nm, and a substantial increase in both ϕ_F (from 0.18 to 0.68) and τ_F (from 3.0 to 5.6 ns). There is a sharpening and intensification of the absorption and fluorescence bands on formation

of the dicationic species (Figure 3) and a corresponding increase in k_{RAD} from 6.0×10^7 to $1.2\times10^8\ s^{-1}$. However, the titration clearly proceeds by way of an intermediate species that bears the hallmarks of the monoprotonated species (Figure 4).

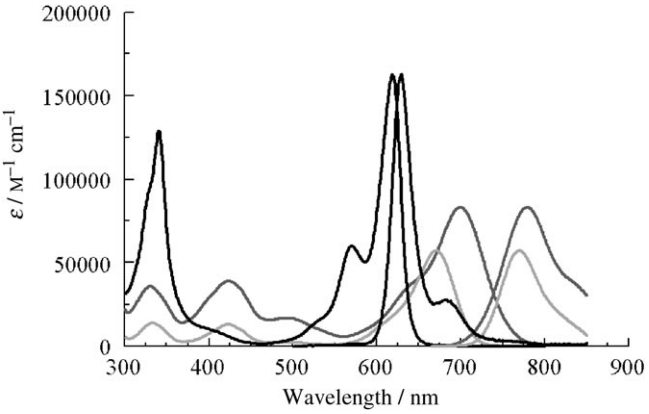

Figure 3. Absorption and fluorescence spectra recorded for **2** at different stages of protonation: neutral species (dark grey curve), monocationic species (light grey curve) and dicationic species (black curve) in CH_3CN.

Thus, stepwise addition of HCl to **2** in CH_3CN leads to the progressive replacement of the strong absorption band centered at 700 nm with a new band centered at 670 nm (Figure 4). This latter band is relatively broad and retains a significant amount of charge-transfer character. There are several clear isosbestic points. Further addition of HCl results in the loss of the 670 nm band and the concomitant evolution of an absorption band centered at 620 nm. No further changes occur on addition of excess acid, but there are at least three evident isosbestic points. The 620 nm band is notably narrower and more intense than the original 700 nm band and is taken to be indicative of the loss of charge-transfer character. There are accompanying changes in the near-UV region. The absorption spectra derived for the mono- and diprotonated species are comparable to those observed for the corresponding N-methylated analogues (Table 1). Similar absorption spectral changes were seen when the proton source was CF_3COOH and in CH_2Cl_2.

The titration was also followed by fluorescence spectroscopy (Figure 5). For **2** in CH_3CN, the fluorescence maximum lies at 785 nm and corresponds to a Stokes' shift of 1630 cm^{-1}. Addition of small amounts of HCl causes the fluorescence intensity to decrease markedly and, although difficult to see by eye, there is a shift in the emission maximum to 772 nm. On further addition of HCl, the emission maximum moves to 630 nm and the intensity grows steadily. The 630 nm band is clearly due to the diprotonated species, for which the Stokes' shift is only 280 cm^{-1}. As noted for **3b**, this species possesses little if any charge-transfer character. The intermediate species can be attributed to the monoprotonated material, for which the Stokes' shift is increased to 1970 cm^{-1}, and that retains a relatively broad spectral profile

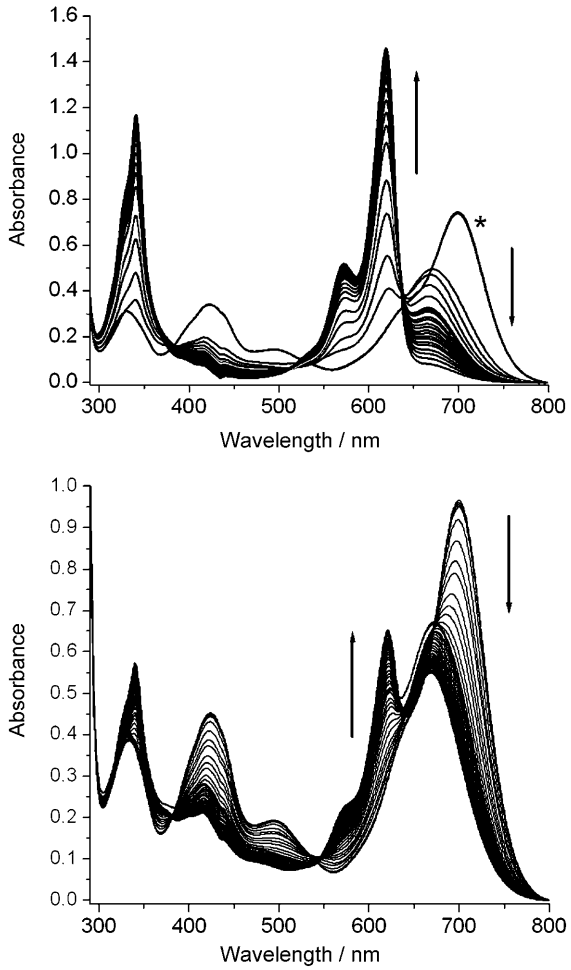

Figure 4. Titration of **2** in CH_3CN with HCl. The lower panel shows the initial part of the titration, while the upper panel focuses on the second protonation step. The curve labeled with an asterix corresponds to the starting solution. Sufficient HCl is then added to convert the neutral species to the monocation so that the second protonation can be followed.

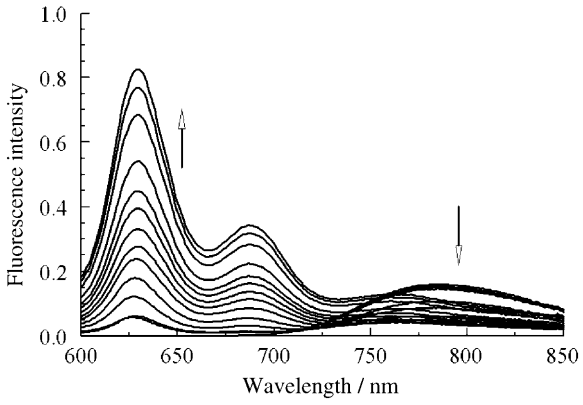

Figure 5. Fluorescence spectra recorded for **2** after progressive addition of HCl in CH_3CN (excitation was made at the isosbestic point at 548 nm).

consistent with considerable charge-transfer character. Thus, a major consequence of diprotonation is that the dipole

moment (i.e., the Stokes' shift) vanishes. Protonation of the first N atom removes that particular donor site and should thereby increase the dipole moment. This, in turn, will increase the state of hybridization of the second N atom, which will become more difficult to protonate. It is recognized, however, that the ammonium ion exerts an inductive effect that will keep the dipole moment to a modest level. It is this concerted behavior that allows separation of the successive protonation steps. Although there will be an associated electrostatic effect, the two N atoms are too far apart for this to be the primary cause of the disparate reactivity of these donor sites.

Analysis of the absorption spectral changes caused by addition of HCl in CH_3CN in terms of two successive protonation steps gives pK_a values of 3.04 and 5.10, respectively (see Supporting Information Figures S6 and S7). These are averaged values obtained by fitting the data to conventional pK_a transitions by using SPECFIT and also by using the ratiometric method,[36] taking advantage of the well-preserved isosbestic points. In the former case, the entire spectral window was used, but in the latter case data analysis was restricted to ten individual wavelengths. The fluorescence titration data were analyzed using SPECFIT to give pK_a values of 3.0 and 5.2. Unfortunately, the first pK_a is difficult to assess by fluorescence spectroscopy, because it is on the limit of our detection window, but the second protonation step can be followed easily by the appearance of emission around 630 nm. Overall, the derived pK_a values for the two steps are consistent among the various measurements. Monoprotonation, which gives rise to only modest spectral changes, involves a relatively high pK_a value and is switched-on at quite low concentrations of acid. In contrast, diprotonation induces substantial spectral shifts, but demands moderately high acid concentrations. It is notable that the first pK_a value is higher than that determined for a derivative of **1**, despite the comparable experimental conditions.[28] This behavior might have been expected in view of the significantly lower dipole moment exhibited by **2**, which will favor a higher pK_a value. Even so, it is a fairly large change in reactivity that serves to demonstrate the sensitivity of the protonation process. Likewise, the difference in pK_a values noted for addition of one and two protons indicates that the ammonium cation exerts a strong effect on the electronic properties of the molecule.

Covalent attachment to porous beads: To fix the dye to a macroscopic support it proved necessary to master the chemistry of the iodo function without harming the fluorescence properties. Thus, cross-coupling of **2** with ethyl hept-6-ynoate by using Pd^0 as catalyst under mild conditions afforded **4** in excellent yield. Hydrolysis of the ester was straightforward and gave **5** in quantitative yield. In an effort to link this dye to Amberzyme Oxirane™ beads, which have a low dispersity with average diameter of 200 μm, we first treated the oxirane-functionalized beads with excess 1,3-diaminopropane in anhydrous THF in the presence of $LiClO_4$.[38] After vigorous shaking, followed by subsequent drying and washing, the beads were isolated by sieving. Linkage of the dye to the beads was inspired by peptide synthesis,[37] and was made feasible by using a solution of **5** (1.3 mmol), *N*-(3-dimethylaminopropyl)-*N*′-ethyl-carboimide hydrochloride (10 mol%) and 5-dimethylaminopyridine (15 mol%) in a mixture of THF (5 mL) and CH_3OH (1 mL). After shaking overnight, analysis of the solution by absorption spectrophotometry allowed us to conclude that 42 mol% of **5** had been grafted onto 40 mg of beads. This corresponds to an approximate loading of 13 nmol of dye per bead. After prolonged washing, the resultant beads were green. In contrast, blank experiments carried out with dye and Amberzyme Oxirane beads, but without prior treatment with 1,3-diaminopropane, revealed no surface loading and no color change. The specific surface area, as determined by the chemisorption of N_2, of the microspheres is about 220 m^2g^{-1} and the cumulative surface area of the pores is about 190 m^2g^{-1}, clearly corresponding to highly porous material. Scanning electron microscopy (SEM) showed the mean diameter to be about 200 μm. The size distribution of the pores lies in the range of 50 to 100 nm, indicating that the dye can be bound to both outer and inner surfaces. In some instances, SEM shows the presence of strings of larger pores (Figure 6). This level of loading is reproducible and the bound dye is stable with respect to leaching from the surface after prolonged exposure in air to light or solvent.

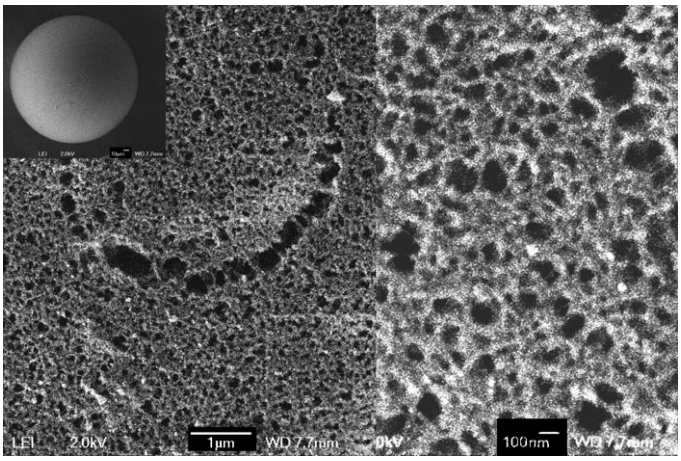

Figure 6. Examples of SEM photographs of the functionalized bead surface (left) and a zoom of the surface showing the pore distribution (right).

Examination of the capability of the loaded beads to detect trace quantities of acid present in a gas stream is illustrated in Figure 7. The beads are packed into an open-ended microcapillary and exposed to the gas flow. On illumination with a 365 nm UV lamp, the fluorescence of the dye adhered to the surface of the beads lies at 770 nm, but could not observed by the naked eye. Instead, the beads appear violet-blue due to very weak background fluorescence from the treated surface (Figure 7b); note untreated beads do not fluoresce. When the gas flow was spiced with a

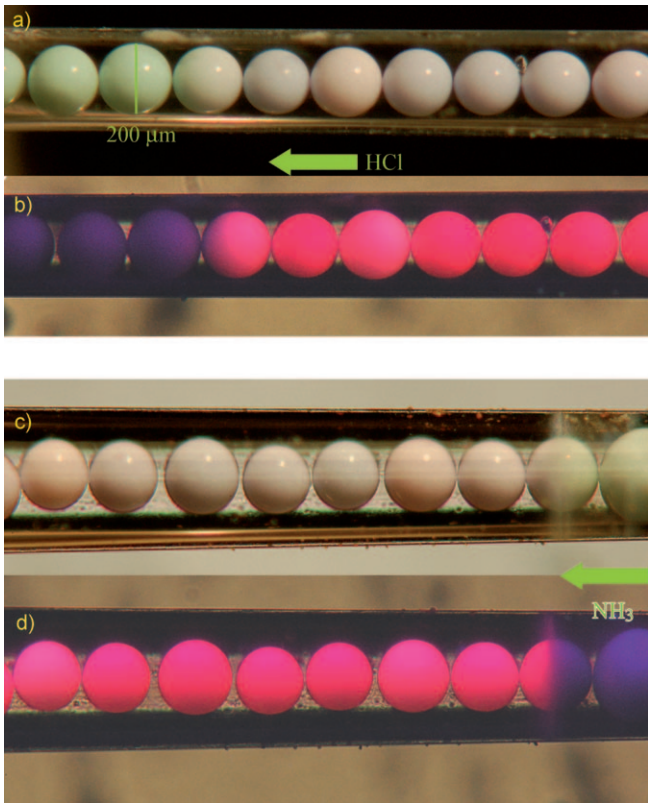

Figure 7. Open-ended capillary tube packed with macroscopic beads functionalized with 13 nmol of **5** as observed with an optical microscope at 4× magnification. From the top: a) Exposure of the beads to a current of air loaded with a trace of HCl gas. b) The same capillary tube but observed by fluorescence with excitation at 365 nm. c) Exposure of the protonated beads to a current of air loaded with a trace amount of NH_3. d) The same capillary tube but observed by fluorescence with excitation with a non-filtered 365 nm bench UV lamp. Note, the blue color observed in b) and d) is due to weak inherent fluorescence from surface-treated beads. Fluorescence from the green dye occurs around 800 nm and cannot be observed by the naked eye.

trace of HCl, the beads instantaneously turned blue and there was concomitant appearance of an intense red fluorescence (Figure 7c). The lower limit for detection of HCl in air, as determined by the naked eye for illumination with a low intensity UV source, lies in the 400 to 800 ppb range. The uncertainty is due to the very low concentration of acid. Each experiment was repeated five times and the quoted range represents the lower and upper limits of detection that were encountered. Furthermore, when the gas flow contains trace amounts of ammonia, the blue beads revert to their original color and the red fluorescence disappears (Figure 7).

This on–off color switching is stable for at least one year and there was no decrease in efficacy after more than ten complete cycles carried out in rapid succession. The detection limit for ammonia is between 60 and 120 ppb by using the same "naked eye" approach. The resultant NH_4Cl deposits on the capillary walls or is removed by the gas flow. This detection limit was improved by two orders of magnitude by using routine optical spectroscopic equipment, most notably a laser diode as excitation source and a photocell as detector, even without signal amplification. Systematic exposure of the beads to aqueous solutions allowed the pK_a for the acid/base transition to be identified as lying in the 2.4 to 2.6 pH range, as determined by the "naked-eye". Clearly, this refers to addition of the second proton and is reasonably consistent with the results of the pH titrations carried out for **2** in acetonitrile.

The same concept can be applied to the detection of trace amounts of highly toxic chemicals and to vesicant warfare gases, provided they contain acidic or alkylating groups. Thus, loaded beads packed into a glass capillary and illuminated at 365 nm display pronounced fluorescence at around 800 nm that can be monitored with a photocell, but is outside of the range detectable by the human eye (Figure 8).

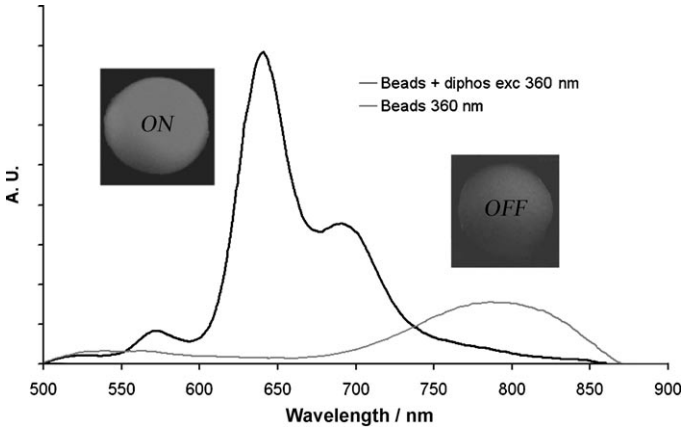

Figure 8. Steady-state fluorescence spectra recorded for beads packed into a quartz capillary tube; normal beads in air (grey curve) and beads exposed briefly to a trace amount of diphosgene vapor (black curve). The inserts show a single bead as observed by an optical fluorescence microscope with excitation at 365 nm before and after exposure to diphosgene.

However, when trace amounts of diphosgene were allowed to enter the capillary tube there was an immediate color change from green to blue.[39] This transition was accompanied by the appearance of intense red fluorescence; this emission is centered at 650 nm and can be seen easily by the human eye (Figure 8). It was not possible to estimate the lower detection level for phosgene, because of the difficulty in handling this material under quantitative conditions in our laboratory. The lower level, however, is at least as good as that found for HCl. This protocol can be adapted for facile detection of other highly toxic materials such as nitrogen and sulfur mustard gases, phosphine, arsines, and HCN.

The visual detection process (red fluorescence) is unaffected by humidity or even when the gas stream is saturated with water. Hence, when the beads are dispersed in aqueous solution the on–off detection process continues to operate on addition of trace amounts of HCl or HCOOH. The use of triethylamine or piperidine vapors in place of ammonia is also effective in extinguishing the red fluorescence. We em-

phasize, however, that there is no selectivity for any particular acid or base in either solution or gaseous states.

Conclusion

The current set-up has been designed to operate as a simple saturation-type optical detector for monitoring the presence of trace amounts of acidic or electrophilic pollutants. The dye-coated beads are highly stable and exhibit a green-to-blue color transformation on exposure to acid; the reverse process is available for the detection of bases, such as ammonia or organic amines, simply by pre-exposure of the beads to acid. There is a concomitant change in the fluorescence maximum from 800 to 650 nm; this has the effect of moving the emission from the far-red to the visible region. By using a capillary tube, the device is easily saturated and this makes for facile on–off sensing that can be followed by the naked eye. The green to blue color change is nicely complemented by the emergence of an intense red emission, thereby fulfilling the basic requirement for orthogonal sensing. Under spectroscopic conditions, the most important detection mode involves the parallel monitoring of the absorbance change at 720 nm and the accompanying modulation of the fluorescence intensity at 650 nm. An advantage of the capillary tube is that the dye is quickly saturated, but many facile modifications are possible. Thus, the glass capillary can be replaced with a porous tube and used to monitor aerosols or circulating liquids. At the present stage, the sensor is not specific towards the nature of the acid or base, but it should be emphasized that this prototype could be chemically modified at the aromatic amine site so as to produce shape-specific molecular pockets[40] able to recognize certain species.

The main motivation for synthesizing a BODIPY-based dye equipped with two vinylic arms relates to the positioning of the relevant optical absorption and fluorescence maximum. This represents a deliberate attempt to generate the most visual changes upon contacting the beads with the substrate. An unexpected feature of this strategy relates to the relative inactivation of the second nitrogen atom caused by alkylation or protonation of the first anilino N atom. This leads to a marked disparity in the respective pK_a values. Although reaction at the first N atom does not cause dramatic spectral changes it is notable that the pK_a is sufficiently high for sensitive detection of substrates at low concentration. The second pK_a value is such that high concentrations of substrate are required. In terms of sensor technology, this situation could be exploited to develop dual-purpose detectors. Here, reaction at the first N atom would send a warning signal to the operator to the effect that low concentrations of the substrate had entered the system. Reaction at the second N atom would be used to signal that the process must be shut down. In a chemical sense, the disparate pK_a values relate to a changeover from the strongly donating nature of the amino group to the inductive effect inherent to the ammonium group. The effect is amplified by the V-shaped geometry of **2**, in which the initial electronic system is best represented as push–pull–push. After monoalkylation, or monoprotonation, the electronic system becomes push–pull–pull with a concomitant enhancement of the dipole moment.

Experimental Section

Synthesis and characterization of compounds 1 and 2: Prepared according to previously published procedures for isolation of monosubstituted compounds,[26] from 8-(4-phenyliodo)-tetramethyldifluoroboradipyrromethene (500 mg, 1.11 mmol) and 4-dimethylaminobenzaldehyde (362 mg, 2.44 mmol) in a mixture of toluene (20 mL) and piperidine (0.5 mL) containing a single crystal of *p*-TsOH at 120 °C for 1 d. Chromatography on silica gel, eluting with a gradient of dichloromethane-petroleum ether (*v*/*v* 30:70) to dichloromethane, gave **1** (168 mg, 26%) as a deep-blue solid and **2** (459 mg, 58%) as a deep-green solid after recrystallization from a dichloromethane–cyclohexane mixture.

Data for ***1***: ^{1}H NMR ([D$_6$]DMSO, 400 MHz): δ = 7.76 (d, ^3J = 17.2 Hz, 1H), 7.62 (d, ^3J = 8.8 Hz, 2H), 7.44 (d, ^3J = 17.2 Hz, 1H), 7.38 (d, ^3J = 8.8 Hz, 2H), 7.12 (d, ^3J = 8.7 Hz, 2H), 6.82 (d, ^3J = 8.7 Hz, 2H), 6.75 (s, 1H), 6.04 (s, 1H), 3.14 (s, 6H), 2.62 (s, 3H), 1.51 (s, 3H), 1.48 ppm (s, 3H); ESI-MS in CH$_3$OH + 1% TFA: *m*/*z* (%): 582.2 (100) [*M*+H]$^+$; elemental analysis calcd (%) for $C_{28}H_{27}N_3IBF_2$: C 57.86, H 4.68, N 7.23; found: C 57.57, H 4.44, N 7.00.

Data for ***2***: ^{1}H NMR ([D$_6$]DMSO, 400 MHz): δ = 7.93 (d, ^3J = 8.3 Hz, 2H), 7.47 (d, ^3J = 8.8 Hz, 4H), 7.43 (d, ^3J = 17.1 Hz, 2H), 7.30 (d, ^3J = 17.1 Hz, 2H), 7.24 (d, ^3J = 8.3 Hz, 2H), 6.89 (s, 2H), 6.79 (d, ^3J = 8.8 Hz, 4H), 3.00 (s, 12H), 1.43 ppm (s, 6H); ESI-MS in CH$_3$OH + 1% TFA: *m*/*z* (%): 713.2 (100) [*M*+H]$^+$; elemental analysis calcd (%) for $C_{37}H_{36}N_4IBF_2$: C 62.38, H 5.09, N 7.86; found: C 62.12, H 4.83, N 7.57.

Synthesis and characterization of compounds 3a and 3b: The green dye **2** (100 mg, 0.14 mmol) dissolved in acetonitrile (10 mL) was allowed to react with CH$_3$I (3 mL) for 48 h at RT. The course of reaction was followed by TLC on silica gel, using a mixture of acetonitrile/water as eluant (85:15). After disappearance of the starting material, the deep-blue solution was evaporated to dryness and dissolved in a mixture of water/methanol. A tenfold excess of KPF$_6$ dissolved in water was added dropwise, resulting in precipitation of the salt. The organic phase was evaporated to dryness and the precipitate was washed with water and diethyl ether. Purification was ensured by column chromatography on alumina using acetonitrile/water as solvent 85:15 v/v. The first compound to be eluted was **3a**, which, after recrystallization in acetone, was isolated as a greenish-blue solid (26 mg, 20%). The second compound to be eluted from the column was recrystallized by slow evaporation of acetone from a mixture of acetone/cyclohexane to give **3b** as deep-blue crystals (80 mg, 55%).

Data for ***3a***: ^{1}H NMR ([D$_6$]DMSO, 400 MHz): δ = 7.72 (d, ^3J = 17.1 Hz, 2H), 7.60 (d, ^3J = 8.8 Hz, 4H), 7.39 (d, ^3J = 17.1 Hz, 2H), 7.41 (d, ^3J = 8.8 Hz, 4H), 7.15 (d, ^3J = 8.6 Hz, 2H), 6.89 (d, ^3J = 8.6 Hz, 2H), 6.84 (s, 1H), 6.17 (s, 1H), 4.38 (s, 9H), 3.10 (s, 6H), 1.54 (s, 3H), 1.49 ppm (s, 3H); ESI-MS in CH$_3$CN: *m*/*z* (%): 727.3 (100) [*M*−PF$_6$]$^+$; elemental analysis calcd (%) for $C_{38}H_{39}N_4IBF_2PF_6$: C 52.32, H 4.51, N 6.42; found: C 52.52, H 4.66, N 6.57.

Data for ***3b***: ^{1}H NMR ([D$_6$]DMSO, 400 MHz): δ = 7.97 (d, ^3J = 8.4 Hz, 2H), 7.49 (d, ^3J = 8.7 Hz, 4H), 7.45 (d, ^3J = 17.0 Hz, 2H), 7.26 (d, ^3J = 17.0 Hz, 2H), 7.17 (d, ^3J = 8.4 Hz, 2H), 6.99 (s, 2H), 6.83 (d, ^3J = 8.7 Hz, 4H), 4.23 (s, 18H), 1.54 ppm (s, 6H); ESI-MS in CH$_3$CN: *m*/*z* (%): 887.2 (80) [*M*−PF$_6$]$^+$, 371.1 (100) [*M*−2PF$_6$]$^{2+}$; elemental analysis calcd (%) for $C_{39}H_{42}N_4IBF_2P_2F_{12}$: C 45.37, H 4.10, N 5.43; found: C 45.22, H 3.89, N 5.29.

Synthesis and characterization of compound 4: Compound **4** Prepared from compound **2** (100 mg, 0.140 mmol) and HC≡CC$_4$H$_8$COOEt (32 mg, 0.210 mmol) in a mixture of THF (5 mL), diisopropylamine (2 mL), [Pd(PPh$_3$)$_2$Cl$_2$] (6 mg) and CuI (6 mg) at RT for one night. After that time,

the mixture was evaporated to dryness and treated with water (5 mL), before being extracted with dichloromethane (3×50 mL). The organic phase was dried over $MgSO_4$ and evaporated to dryness. The pure compound was obtained by chromatography on silica gel, eluting with dichloromethane-petroleum ether (*v/v* 60:40) to give **4** as a deep-green solid (100 mg, 97%) after recrystallization from a dichloromethane–cyclohexane mixture. ^{1}H NMR ([D$_6$]DMSO, 400 MHz): δ=7.89 (d, ^3J= 8.2 Hz, 2H), 7.43 (d, ^3J=8.7 Hz, 4H), 7.37 (d, ^3J=16.9 Hz, 2H), 7.28 (d, ^3J=16.9 Hz, 2H), 7.18 (d, ^3J=8.2 Hz, 2H), 6.82 (m, 6H), 4.17 (q, ^3J= 7.1 Hz, 2H), 2.94 (s, 12H), 2.38–2.25 (m, 4H), 1.89–1.65 (m, 4H), 1.42 (s, 6H), 1.28 ppm (t, ^3J=7.1 Hz, 3H); ESI-MS: *m/z* (%): 739.2 (100) $[M+H]^+$, 719.3 (20) $[M-F]^+$; elemental analysis calcd (%) for $C_{46}H_{49}N_4O_2BF_2$: C 74.79, H 6.69, N 7.58; found: C 74.52; H 6.39; N 7.27.

Synthesis and characterization of compound 5: Saponification of **4** (70 mg, 0.09 mmol) in a mixture of THF (5 mL) and methanol (3 mL) was carried out using NaOH at 60°C for 16 h. The course of reaction was followed by TLC, clearly showing the formation of a green polar compound at the expense of the nonpolar starting material. On completion of the reaction, the pH was adjusted to 7.0 by using a solution of dilute HCl. The target acid was extracted with dichloromethane and the organic phase dried over $MgSO_4$. The analytically pure sample was obtained after recrystallization from a mixture of dichloromethane, methanol (trace) and cyclohexane providing of **5** as deep-green crystals (63 mg, 99%). ^{1}H NMR ([D$_6$]DMSO, 400 MHz): δ=7.94 (d, ^3J=8.3 Hz, 2H), 7.47 (d, ^3J=8.7 Hz, 4H), 7.39 (d, ^3J=17.2 Hz, 2H), 7.34 (d, ^3J=17.2 Hz, 2H), 7.27 (d, ^3J=8.3 Hz, 2H), 6.89 (m, 6H), 3.03 (s, 12H), 2.47–2.18 (m, 4H), 1.92–1.67 (m, 4H), 1.50 ppm (s, 6H); ESI-MS: *m/z* (%): 711.2 (20) $[M+H]^+$, 691.3 (100) $[M-F]^+$; elemental analysis calcd (%) for $C_{44}H_{45}N_4O_2BF_2$: C 74.36, H 6.38, N 7.88; found: C 74.19, H 6.17, N 7.62.

General conditions: 400 MHz ^{1}H NMR spectra were recorded at room temperature by using the residual proton resonances in deuterated solvents as internal references. Chromatographic purification was conducted using Silica gel Si-60 (40–63 μm). Thin-layer chromatography (TLC) was performed on silica gel plates coated with fluorescent indicator. All mixtures of solvents are given as v/v ratios. Synthetic details, including compound characterization, are given in the Supporting Information.

Spectroscopic measurements: Electronic absorption and emission spectra were measured under ambient conditions using commercial instruments. Fluorescence spectra were recorded with a Yvon–Jobin Fluorolog tau-3 equipped with a near-IR photodiode detector and with gratings blazed at 700 nm. Spectral imperfections were corrected by reference to a standard lamp. Solvents for spectroscopy were spectroscopic grade and were used as received after checking for impurities. A wide variety of excitation wavelengths were used, according to the species under investigation. Spectral titrations were carried out with excitation at isosbestic points. Fluorescence quantum yields were measured relative to Cresyl Violet for **2**[41] and tetramethoxy-bis-isoindolodipyrromethene-difluoroborate for **2**, **4**, and **5**.[42] Luminescence lifetimes were measured by using the time-correlated, single-photon counting mode coupled to a Stroboscopic system. The excitation source was a thyratron-gated flash lamp filled with nitrogen gas. No filter was used for the excitation. The instrumental response function was determined with a scattering solution.

X-ray studies: Crystallographic measurements were carried out at 293(2) K on a Nonius kappa-CCD diffractometer by using monochromatic graphite $Mo_{K\alpha}$ radiation (λ=0.71073 Å). Accurate unit cell parameters and orientation matrices were obtained from least-squares refinement. Reflections were processed with Denzo[42] and scaled in Scalepack[43] after post-refinement of the unit cell parameters. The structures were solved by direct methods (SHELXS 97) and refined by full-matrix, least-squares techniques on F^2 using SHELXL 97.[44] Differences in diffraction power were observed between thin-plate crystals for compound **1** and **2**, resulting in C–C bond length precision about three times better for the molecular structure of compound **1** (0.006 vs 0.018 Å). Details of the data collection and structure refinements are given in the Supporting Information. Quantum Chemical calculations were performed with SPARTAN version 06 (Wavefunction Inc).

Functionalization of the polyacrylate beads (AMBERZYME® OXIRANE from Rohm and Haas, France): The Amberzyme oxirane beads **I** (1 g, co-polymer containing ethyleneglycoldimethacrylate 70% and glycidylmethacrylate 30%) were suspended in a solution of anhydrous THF (5 mL), diaminopropane (5 mL), and $LiClO_4$ (200 mg) and shaken overnight at RT. The deposited white beads were washed with THF, dichloromethane, methanol, and diethyl ether. The resultant surface-modified beads **II** were dried under high vacuum overnight.

Dye **5** (2 mg) was dissolved in a solution containing THF (5 mL), methanol (1 mL), *N*-(3-dimethylaminopropyl)-N′-ethyl-carboimide hydrochloride (0.3 mg, 10 mol%) and 4-dimethylaminopyridine (0.2 mg, 15 mol%). Beads **II** (40 mg) were added to this fresh mother liquor (3 mL), and the resultant mixture was shaken for 8 h. After decantation, the beads were washed copiously with THF (2×15 mL), dichloromethane (2×25 mL), methanol (15 mL), and diethyl ether (15 mL). The resultant beads were green and the absorbance of the residual solution was used to determine the level of dye loaded onto the surface. On average, a single bead contains 13 nmol of the dye (about 2 μg per bead of 200 μm size).

Blank experiment: Beads **I** (40 mg) were added to the fresh mother liquor (3 mL), and the resulting mixture was shaken for 8 h and treated as described above. The recovered beads remain white and the solution has the same concentration of dye as the mother liquor, according to absorption spectroscopy.

Gas detection: To determine the "naked eye" detection limit for gaseous HCl (99.9% purity) and ammonia (99% purity), a Schlenk style technique was developed. Pure gases were stored in a calibrated flask, degassed under high vacuum before being filled at atmospheric pressure and room temperature. The flask was sealed with a syringe valve. Known volumes of pure gas were withdrawn by using gas-tight syringes and diluted with known quantities of dry air. Each experiment was repeated five times and the quoted detection range corresponds to the lower and upper limits of the abilities of different observers to detect the color changes using both absorption and fluorescence approaches.

Spectroscopic titrations: Absorption and fluorescence spectral titrations were made with solutions of **2** in CH_3CN following addition of standard solutions of HCl in CH_3CN. A known volume of the dye solution was stirred at 20°C and aliquots of HCl solution added by means of a calibrated syringe. The solution was equilibrated before recording the spectrum. Several different concentrations of acid were used as the titration progressed. The results were corrected for dilution and analyzed with SPECFIT. Each titration was repeated four times. Corresponding titrations were carried out with trifluoroacetic acid in both CH_3CN and CH_2Cl_2.

Acknowledgement

We thank the CNRS, ANR and the University Louis Pasteur of Strasbourg for financial support of this work. Dr. J. Hawecker (Rohm and Haas, France) is thanked for help with the beads. Drs. T. Dintzler and D. Begin (LMSPC, Strasbourg) are thanked for the SEM and BET measurements.

[1] a) A. P. De Silva, H. Q. N. Gunaratne, T. Gunnlaugsson, A. J. M. Huxley, C. P. McCoy, J. T. Rademacher, T. E. Rice, *Chem. Rev.* **1997**, *97*, 1515–1566; b) *Chemosensors of Ion and Molecular Recognition* (Eds.: J.-P. Desvergne, A. W. Czarnik) Kluwer, Dordrecht, **1997**; c) *Chemical Sensors and Biosensors for Medical and Biological Applications* (Ed.: U. E. Spichiger-Keller), Wiley-VCH, Weinheim, **1998**; d) P. D. Beer, P. A. Gale, *Angew. Chem.* **2001**, *113*, 502–532; *Angew. Chem. Int. Ed.* **2001**, *40*, 486–516; e) H. Tsukube, S. Shinoda, *Chem. Rev.* **2002**, *102*, 2389–2404; f) *Molecular Fluorescence: Principles and Applications* (Ed.: B. Valeur), Wiley-VCH, Weinheim, **2002**.

[2] See, for example: a) *Coord. Chem. Rev.* **2000**, *205*, 1–232 (whole issue); b) A. B. Ellis, D. R. Walt, *Chem. Rev.* **2000**, *100*, 2477–2738;

c) C. Bargossi, M. C. Fiorini, M. Montalti, L. Prodi, N. Zaccheroni, *Coord. Chem. Rev.* **2000**, *208*, 17–32; d) L. Prodi, F. Bolletta, M. Montalti, N. Zaccheroni, *Coord. Chem. Rev.* **2000**, *205*, 59–83; e) A. P. De Silva, G. D. Mclean, T. S. Moody, S. M. Weir in *Handbook of Photochemistry and Photobiology Vol. 3* (Ed.: H. S. Nalwa), American Institute of Physics, Stevenson Ranch **2003**, pp. 217–238; f) P. Jiang, Z. Guo, *Coord. Chem. Rev.* **2004**, *248*, 205–229; g) L. Prodi, *New J. Chem.* **2005**, *29*, 20–31.

[3] a) O. S. Wolfbeis in *Fiber Optic Chemical Sensors and Biosensors II*, CRC, Boca Raton, **1991**; b) P. Simon, F. Kvanik in *Optical Sensors for Industrial, Environmental and Clinical Applications* (Eds.: R. Narayanaswamy, O. S. Wolfbeis), Springer, Heidelberg, **2003**, pp. 441–465.

[4] M. G. Baron, R. Narayanaswamy, S. C. Thorpe, *Sens. Actuators B* **1996**, *34*, 511–515.

[5] K. Nakagawa, T. Kitagawa, Y. Sadaoka, *Sens. Actuators B* **1998**, *52*, 10–14.

[6] H. Supriyatno, M. Yamashita, K. Nakagawa, Y. Sadaoka, *Sens. Actuators B* **2002**, *85*, 197–204.

[7] E. Wang, K.-F. Chow, W. Wang, C. Wong, C. Yee, A. Persad, J. Mann, A. Bocarsly, *Anal. Chim. Acta* **2005**, *534*, 301–306.

[8] R. Gvishi, R. Reisfeld, *Chem. Phys. Lett.* **1989**, *156*, 181–186.

[9] Y. Sadaoka, Y. Sakai, Y. Murata, *Talanta* **1992**, *39*, 1675–1679.

[10] Y. Sadaoka, Y. Sakai, M. Yamada, *J. Mater. Chem.* **1993**, *3*, 877–881.

[11] T. A. Dickinson, J. White, J. S. Kauer, D. R. Walt, *Nature* **1996**, *382*, 697–700.

[12] E. Scorsone, S. Christie, K. C. Persaud, F. Kvasnik, *Sens. Actuators B* **2004**, *97*, 174–181.

[13] E. Pringsheim, E. Terpetsching, O. S. Wolfbeis, *Anal. Chim. Acta* **1997**, *357*, 247–252.

[14] a) M. Mazur, P. Krysinski, K. Jackowska, *Thin Solid Films* **1998**, *330*, 167–172; b) L. Bansal, M. El-Sheriff, J. Yuan, *Sensors* **2007**, *7*, 3100–3118.

[15] A. T. Canada, L. R. Allain, D. B. Beach, Z. Xue, *Anal. Chem.* **2002**, *74*, 2535–2540.

[16] A. Loudet, K. Burgess, *Chem. Rev.* **2007**, *107*, 4891–4932.

[17] a) G. Ulrich, R. Ziessel, A. Harriman, *Angew. Chem.* **2008**, *120*, 1202–1219; Angew. Chem. Int. Ed. **2008**, 47, 1184–1201; b) R. Ziessel, G. Ulrich, A. Harriman, *New J. Chem.* **2007**, *31*, 496–501.

[18] F. López-Arbeloa, J. Banuelos Prieto, V. Martinez Martinez, T. Arbeloa Lopez, I. Lopez Arbeloa, *ChemPhysChem* **2004**, *5*, 1762–1771.

[19] *The Handbook—A Guide to Fluorescent Probes and Labelling Technologies* (Ed.: R. P. Haughland), Invitrogen/Molecular Probes, **2005**.

[20] J. L. Bricks, A. Kovalchuk, C. Trieflinger, M. Nofz, M. Büschel, A. I. Tolmachev, J. Daub, K. Rurack, *J. Am. Chem. Soc.* **2005**, *127*, 13522–13529.

[21] A. Coskun, E. U. Akkaya, *J. Am. Chem. Soc.* **2006**, *128*, 14474–14475.

[22] A. Harriman, G. Izzet, R. Ziessel, *J. Am. Chem. Soc.* **2006**, *128*, 10868–10875.

[23] R. Y. Lai, A. J. Bard, *J. Phys. Chem. B* **2003**, *107*, 5036–5042.

[24] W. Qin, M. Baruah, M. van De Auweraer, F. C. Schryver, N. Boens, *J. Phys. Chem. A* **2005**, *109*, 7371–7384.

[25] G. Ulrich, C. Goze, M. Guardigli, A. Roda, R. Ziessel, *Angew. Chem.* **2005**, *117*, 3760–3764; *Angew. Chem. Int. Ed.* **2005**, *44*, 3694–3698.

[26] C.-W. Wan, A. Burghart, J. Chen, F. Bergström, L. B.-A. Johansson, M. F. Wolford, T. G. Kim, M. R. Topp, R. M. Hochstrasser, K. Burgess, *Chem. Eur. J.* **2003**, *9*, 4430–4441.

[27] a) R. P. Haughland, H. C. Kang, U.S. Patent 4.74.339, **1988**; b) K. Rurack, M. Kollmansberger, J. Daub, *New J. Chem.* **2001**, *25*, 289–292; c) Z. Dost, S. Atilgan, E. U. Akkaya, *Tetrahedron* **2006**, *62*, 8484–8488; d) S. Atilgan, Z. Ekmekci, A. L. Dogan, D. Guc, E. U. Akkaya, *Chem. Commun.* **2006**, 4398–4400.

[28] M. Baruah, W. Qin, C. Flors, J. Hofkens, R. A. L. Vallée, D. Beljonne, W. M. Van de Auweraer, M. De Borggraeve, N. Boens, *J. Phys. Chem. A* **2006**, *110*, 5998–6009.

[29] T. Rohand, W. Qin, N. Boens, W. Dehaen, *Eur. J. Org. Chem.* **2006**, 4658–4663.

[30] K. Rurack, M. Kollmannsberger, J. Daub, *Angew. Chem.* **2001**, *113*, 396–399; *Angew. Chem. Int. Ed.* **2001**, *40*, 385–387.

[31] A. Coskun, E. Deniz, E. U. Akkaya, *Org. Lett.* **2005**, *7*, 5187–5189.

[32] Z. Shen, H. Röhr, K. Rurack, H. Uno, M. Spieles, B. Schulz, G. Reck, N. Ono, *Chem. Eur. J.* **2004**, *10*, 4853–4871.

[33] Y.-H. Yu, A. B. Descalzo, Z. Shen, H. Röhr, Q. Liu, Y.-W. Wang, M. Spieles, Y.-Z. Li, K. Rurack, X.-Z. You, *Chem. Asian J.* **2006**, *1*, 176–187.

[34] R. Englman, J. Jortner, *Mol. Phys.* **1970**, *18*, 145–181.

[35] We are well aware that the use of terminology such as pK_a is inappropriate for organic solutions and we do so only to relate our findings to prior literature work. The proton concentrations were determined by dilution of concentrated HCl on the basis of complete dissociation.

[36] a) "Astronomical Data Analysis Software and Systems III": G. A. Kriss, *Astron. Soc. Pac. Conf. Ser.* **1994**, *61*, 437–441; b) W. Qin, M. Baruah, W. M. De Borggraeve, N. Boens, *J. Photochem. Photobiol. A* **2006**, *183*, 190–197.

[37] M. Chini, P. Crotti, F. Macchia, *Tetrahedron Lett.* **1990**, *31*, 4661–4664.

[38] J. Rebek, Jr., D. Feitler, *J. Am. Chem. Soc.* **1974**, *96*, 1606–1607.

[39] Carried out under anhydrous conditions to exclude any traces of acid.

[40] A. Coskun, E. Deniz, E. U. Akkaya, *Tetrahedron Lett.* **2007**, *48*, 5359–5361.

[41] J. Olmsted III, *J. Phys. Chem.* **1979**, *83*, 2581–2584.

[42] G. Ulrich, S. Goeb, A. De Nicola, P. Retailleau, R. Ziessel, *Synlett* **2007**, 1517–1520.

[43] Z. Otwinowski, W. Minor, *Methods Enzymol.* **1997**, *276* 307–326.

[44] G. M. Sheldrick, *Acta Crystallogr. Sect. A* **2008**, *64*, 112–122

Received: September 25, 2008
Published online: December 29, 2008

